Nationaal Lucht- en Ruimtevaartlaboratorium
National Aerospace Laboratory NLR

NLR-TP-2000-447

Perspectives of NLR aeroelastic methods to predict wing/store flutter and dynamic loads of fighter-type aircraft

B.J.G. Eussen, M.H.L. Hounjet, J.J. Meijer, B.B. Prananta and I W. Tjatra

Nationaal Lucht- en Ruimtevaartlaboratorium
National Aerospace Laboratory NLR

NLR-TP-2000-447

Perspectives of NLR aeroelastic methods to predict wing/store flutter and dynamic loads of fighter-type aircraft

B.J.G. Eussen, M.H.L. Hounjet, J.J. Meijer, B.B. Prananta and I W. Tjatra

(alphabetical order)

This report is based on a presentation held at the 22nd ICAS Congress, Harrogate, United Kingdom, 27 August - 1st September, 2000.

The results presented in this technical publication are derived from investigations carried out under contracts awarded by the Netherlands Agency for Aerospace Programmes (NIVR-BRP), the Royal Netherlands Air Force (RBKLu) and the Ministry of Defense (NTP).

Division:	Fluid Dynamics
Issued:	September 2000
Classification of title:	unclassified

Title : Perspectives of NLR Aeroelastic Methods to Predict Wing/Store Flutter and Dynamic Loads of Fighter-Type Aircraft

Author(s) : B.J.G. Eussen, M.H.L. Hounjet, J.J. Meijer, B.B. Prananta and I W. Tjatra (alphabetical order)

date : September 2000

Summary

This paper presents an overview of available aeroelastic methods and the current developments at NLR. The methods for routine flutter prediction are based on the classical linear approach using linear unsteady aerodynamic forces. At some conditions it is found necessary to model nonlinear effects, e.g. prediction of limit cycle oscillations, in which a method based on semi-empirical techniques is employed. To cope with continuously more challenging requirements in the prediction of aeroelastic characteristics, current developments at NLR concentrate on the computational aeroelastic simulation using CFD methods. Relatively mature methods employ potential-flow modeling, while a system with a fluid-structure interaction model and based on the time accurate Euler/Reynolds-Averaged Navier-Stokes equations is currently under development.

Contents

1 Introduction 7

2 Aeroelastic Equations of Motion 10
2.1 Flutter analysis for large number of store configurations 12

3 Frequency Domain Flutter Analysis 13
3.1 Linearized subsonic/supersonic method 14
3.2 Full-potential time-linearized method 15
3.3 Frequency domain aerodynamic data from time-accurate CFD 15

4 Computational Aeroelastic Simulation 17
4.1 Full-Potential flow modeling 17
4.2 Euler/Navier-Stokes flow modeling 18
4.3 Nonlinear semi-empirical model 18
4.4 MIMO-class system identification 20

5 Applications 23

6 Concluding Remarks 27

List of symbols

$[C]$	damping matrix
$[C_{FF}]$	free-free flexibility matrix
C_F	Nonlinear function of ONERA model
Cp	coefficient of pressure
$\boldsymbol{F}_a$	aerodynamic force associated with $\boldsymbol{h}_m$
g	coefficient of proportional damping
$[G]$	interpolation matrix
$\boldsymbol{h}$	displacement
$[K]$	stiffness matrix
k	$\omega L/V$, reduced frequency
L	generalized aerodynamic force (GAF)
$[M]$	mass matrix
q	generalized coordinate
q_∞	dynamic pressure
Q	coefficient of GAF
S	wing area
s	complex Laplace variable
	$s = \sigma + i\omega$
$\boldsymbol{x}$	$[q, \dot{q}]^T$, state variable
α	angle of attack
$\boldsymbol{\phi}$	mode shape
ϕ	velocity potential
ζ	damping factor
ω	circular frequency

Subscripts

E	elastic mode
m	mean value (time-averaged)
R	rigid body mode

This page is intentionally left blank.

1 Introduction

The operation of modern fighter-type aircraft requires careful prediction of possible hazardous flutter instabilities. These data are used to define the operational limit of the aircraft as well as to design the maintenance schedule.

A typical feature of modern fighter aircraft which are expected to carry a wide range of external stores, is the strong variation in mass distributions and concomitant strong variation of dynamic characteristics of the aircraft structure (resonance frequencies, mode shapes). The characteristics depend to a large extent on the inertial parameters of the individual stores and the way in which they are combined into specific configurations. Moreover, during a mission the structural modes, and hence the flutter speed of the aircraft, may change considerably due to consumption of fuel from external tanks and due to the release of stores. The resulting problem of store flutter clearance for a wide range of "different" aircraft is being approached by NLR by means of an efficient combination of calculations, ground resonance tests and flight tests, see figure 1.

As soon as a relatively new mission profile is defined, the flutter clearance activities have to be carried out to investigate the safety of the flight conditions in the mission profile. Since many flutter calculations have to be carried out, involving various stores configurations, linearized flutter calculations are mostly employed, using either linear unsteady aerodynamics or nonlinear transonic aerodynamics.

At a certain condition though, nonlinear transonic aeroelastic phenomena typified as limit cycle oscillations (LCO) may occur. LCO is related to flutter but affects aircraft performance and pilot comfort in a manner similar to buffet. While such transonic LCO instabilities are often a cause for concern, it is important to emphasize as well that subcritical response, or the aeroelastic response of dynamic loads, is equally important and for certain aircraft configurations it may be even more important. Typical conditions of transonic LCO instabilities are moderate angle-of-attack, usually lower than 10 deg and Mach numbers ranging from 0.8 to 1.1. The flow conditions during this type of LCO are characterized primarily by mixed attached/separated flow. Lowly damped structural vibration modes tend to be excited provided they have the proper characteristics to couple with this type of flow. This coupling frequently occurs near flutter boundaries obtained with linear theory.

In response to the need to determine accurately the aeroelastic stability and dynamic loads on fighter-type aircraft in the transonic speed range an investigation was started at NLR in the early

nineties in close cooperation with Lockheed Martin Tactical Aircraft System, Fort Worth, to understand and subsequently predict the nature of LCO experienced by fighter-type aircraft maneuvering at transonic speeds. It consisted of an extensive wind tunnel investigation on oscillating fighter-type wings, followed by the development of semi-empirical aerodynamic and aeroelastic models for prediction of LCO. The prediction method was applied successfully to several fighter configurations and was able to identify correctly those which have encountered LCO. Application of the semi-empirical prediction method, however, is limited to those configurations for which relevant unsteady flow wind-tunnel data are available.

Further, in modern fighter-type aircraft there is a strong potential for interaction between aeroelasticity and high-gain flight control systems leading to aeroservoelasticity. Aeroservoelasticity is a multidisciplinary technology dealing with the interaction of the flexible aircraft structure, the steady and unsteady aerodynamic forces acting on the aircraft, the flight control system and the atmospheric disturbances. Its role and importance are increasing in modern aircraft with a high gain digital flight control system which affects aeroelastic stability and (dynamic) loads.

Because fighter-type aircraft are commonly cleared to fly in a wide variety of external store configurations at different flow conditions, a continuous attention is given to the economization of aeroelastic calculations methods without sacrificing accuracy in the aerodynamic and structural modeling or flow/structure interaction.

Apart from the classical aeroelastic methods, however, computational aeroelastic simulations (CAS) become more and more important. Computational aeroelasticity is a relatively new field emphasizing aeroelastic problems where unsteady and nonlinear aerodynamic loads based on CFD (instead of simple panel methods or measured data) are used to obtain solutions. Important applications are transonic aeroelasticity at low to moderate angles-of-attack, lower speed but high angle-of-attack conditions, etc. Flow/structure interactions in the transonic flow regime can produce alternate separation and reattachment of flow and unusual aeroelastic phenomena that impose limits on the flight envelope.

Discussing computational methods and related issues to calculate aeroelastic characteristics for these aircraft configurations in the subsonic, transonic and supersonic speed regime, it is important to distinguish between the fluid dynamic models and the methods used for their solutions. The fluid dynamic models involved for unsteady aerodynamic computations, depending upon flow conditions, are 1) Classical, linear, small-disturbance equations; 2) Nonlinear potential equations, including both transonic small disturbance and full-potential equations; 3) Euler equations; 4)

Thin-layer Reynolds-Averaged Navier-Stokes equations and 5) Full Reynolds-Averaged Navier-Stokes equations.

In this paper methods for predicting aeroelastic stability (flutter) and dynamic loads for fighter-type aircraft will be highlighted and results will be discussed, in particular:

- Standard flutter stability prediction methods employing subsonic and supersonic panel methods and transonic field panel method for attached flow, applying different aerodynamic modelings.
- Flutter stability prediction methods using characteristic determinant or Nyquist or (well-known) pk-method, including description of flight control system, employing subsonic and supersonic panel methods for attached flow.
- How to calculate efficiently a large number of new store configurations using standard aeroelastic stability prediction methods and advanced methods.
- Numerical aeroelastic simulations applying CFD methods or semi-empirical methods for the more complicated transonic flow conditions.
- Dynamic loads evaluation at high-subsonic/transonic flow conditions during nonlinear flutter and store releases carried out at different maneuvers.

First a short overview of the underlying theory will be described starting with the linearized frequency domain method using several possible unsteady aerodynamic models followed by a time domain method for nonlinear flutter prediction. Then, the current development at NLR concerning the fluid-structure interaction models will be presented. Next, typical routine applications of the methods will be shown. Finally some preliminary results of the current development at NLR will be presented concluded by some final remarks.

2 Aeroelastic Equations of Motion

An adequate description of the displacements of the unrestrained aircraft structure is obtained by taking: 1) the flexibility matrix of the free-free aircraft structure to describe the mean displacements and 2) a set of symmetric and antisymmetric natural vibration modes and the rigid body modes as generalized coordinates. The equations for mean displacements can be expressed in matrix form as:

$$\{\boldsymbol{h}_m\} = [C_{FF}]\,\{\boldsymbol{F}_a\}\,, \tag{1}$$

where $\boldsymbol{h}_m$ is the vector of mean displacements, $\boldsymbol{F}_a$ is the vector of mean aerodynamic loading defined as:

$$\boldsymbol{F}_a = q_\infty \int_{\Delta S} \boldsymbol{n}\; C_{p_m} dS, \tag{2}$$

in which $q_\infty = \frac{1}{2}\rho_\infty V_\infty^2$ is the dynamic pressure, C_{p_m} is the mean pressure distribution. C_{FF} is the "interpolated" flexibility matrix for the aerodynamic control points which is obtained from the flexibility matrix based on the structural control points as:

$$[C_{FF}] = [G][C^s_{FF}][G]^T, \tag{3}$$

where $[G]$ is the interpolation matrix for mapping the displacement at the structural nodes into the aerodynamic control-points. For conservation of energy the aerodynamic force should be mapped into structural nodes using $[G]^T$ [10]. For planar lifting surfaces, the well-known surface spline is usually used. Otherwise a more general approach is applied using in-house developed volume spline methods, see [10].

The mean displacement is defined as the averaged state (time-averaging) of the structure about which (if desired) the linearization of the governing equations is carried out. This displacement can be related to the static deformation of the structure and the rigid body motion of the aircraft (flight mechanics). In the common situation, the spectrum of the mean displacement (relatively low frequency) and the elastic displacement (relatively high frequency) can be separated. One technique to obtain the mean state is by low pass filtering the data with a certain cut-off frequency,

see Meijer and Cunningham, Jr. [18].

The equations of motion are expressed in a matrix form as:

$$\begin{bmatrix} M_R & 0 \\ 0 & M_E \end{bmatrix} \begin{Bmatrix} \ddot{q}_R \\ \ddot{q}_E \end{Bmatrix} + \begin{bmatrix} 0 & 0 \\ 0 & 2\zeta_E M_E \omega_E \end{bmatrix} \begin{Bmatrix} \dot{q}_R \\ \dot{q}_E \end{Bmatrix} + \begin{bmatrix} 0 & 0 \\ 0 & M_E \omega_E^2 \end{bmatrix} \begin{Bmatrix} q_R \\ q_E \end{Bmatrix} = \begin{Bmatrix} L_R \\ L_E \end{Bmatrix}, \tag{4}$$

where M is a generalized mass matrix and q is the vector of generalized coordinates. The indices R and E refer to the rigid body and elastic modes. ζ and ω are the damping factor and natural frequency of each elastic mode and L is the generalized aerodynamic force. Note for clarity that equation(4) governs the dynamic state of the structure about the mean displacement.

The generalized aerodynamic force for the i-th mode is $L_i = q_\infty S Q_i$, where Q is defined as the coefficient of generalized force as:

$$Q_i = \frac{1}{S} \int_S \boldsymbol{\phi}_i \cdot \boldsymbol{n}\, C_p^* \langle t \rangle dS, \tag{5}$$

where $\boldsymbol{\phi}_i$ is the natural mode shape and $C_p^* \langle t \rangle$ is the instantaneous differential pressure distribution over the configuration,

$$C_p^* \langle t \rangle = C_p \langle t \rangle - C_{p_m} \langle t \rangle \tag{6}$$

Note that the pressure distribution C_p^* in expression (5) to (6) is implicitly dependent to the geometry $\boldsymbol{x}\langle t \rangle$ through the time-dependent flow equations.

Finally, the governing aeroelastic equations may be recast into the following matrix equation:

$$[M] \{\ddot{q}\} + [C] \{\dot{q}\} + [K] \{q\} = \{L\langle q, \dot{q} \rangle\}. \tag{7}$$

The influence of mean deformation enters the calculations through a simple iterative matrix multiplication procedure based on equation (1). If the flight conditions are held constant and the change of the mean deformations is within an assigned boundary the latter are frozen.

2.1 Flutter analysis for large number of store configurations

When a large number of store configurations are going to be calculated, Meijer [15] shows that relatively accurate results can be very efficiently obtained by first determining a "fundamental/key configuration" and subsequently perturbing only the mass matrix of this configuration for other configurations. The following equation is used:

$$\left[\tilde{M}\right]\{\ddot{q}\} + [C]\{\dot{q}\} + [K]\{q\} = \{L\langle q, \dot{q}\rangle\}\,. \tag{8}$$

in which $[\tilde{M}]$ is the mass matrix of the current configuration while the other terms belong to the key configuration.

The structural dynamic characteristic of the key configuration, i.e. mode shape, natural frequency, and generalized masses, may be obtained using analytical tools or ground vibration tests. The generalized aerodynamic forces are also calculated only for this key configuration leading to a very efficient method.

3 Frequency Domain Flutter Analysis

Most of the aeroelastic analyses carried out for certification or other purposes are in the frequency domain relying on the linear assumption of the dynamic state with respect to the displacement. However, it should be noted that the dynamic state of the aerodynamic part involved in the analysis may be based on a certain nonlinear fundamental state associated with the mean displacement. The structural part is always assumed to be linear. Assuming the damping is proportional to the stiffness, equation (7) becomes:

$$[M]\,\{\ddot{q}\} + [K(1+ig)]\,\{q\} = \{L\langle\, q, \dot{q}\rangle\}, \tag{9}$$

where g is the coefficient of the proportional damping. In the frequency domain method the motion is assumed to have the form of:

$$\{q\} = \{\hat{q}\}\, e^{st}, \begin{cases} \mathcal{R}(s) < 0 & \text{stable} \\ \mathcal{R}(s) > 0 & \text{unstable} \\ \mathcal{R}(s) = 0 & \text{flutter boundary} \end{cases} \tag{10}$$

where $s = \sigma + i\omega$ is the complex Laplace variable. Several methods for flutter calculations are usually used at the NLR, i.e. the V-g method, pk-method, characteristic determinant method and Nyquist criteria for stability.

In the V-g method the motion is forced to be purely oscillatory (at the flutter boundary, $\sigma = 0$) by adjusting the value of g. Supplementing equation (9) with unsteady aerodynamic forces for oscillatory motion, i.e. $L = L\langle \hat{\boldsymbol{h}}\, e^{ikt} \rangle$ where $k = \omega L/V$ is the reduced frequency and $\hat{\boldsymbol{h}} = \hat{q}\boldsymbol{\phi}$ is the amplitude of the oscillatory motion, an eigenvalue problem can be formulated and solved for $\lambda = (1+ig)/\omega^2$. Flutter velocity is defined as the value of V at which no additional damping is required to force the motion to be oscillatory, i.e. $g = 0$. When the value of g is small the following relation may be used to interpret the results:

$$-\lambda \approx \frac{1}{(\sigma + i\omega)^2}, \qquad \text{for } g \ll 1. \tag{11}$$

In the pk-method the motion may be general ($\sigma \neq 0$) but the aerodynamic force is still kept purely oscillatory. An iteration is required to match the ω of the motion and k used for calculating the aerodynamic force. This matching process enables the possibility to include a transfer function, $[H\langle s\rangle]\{q\}$, e.g. due to (linear) flight control system which depends on ω instead of k, into the governing equations. In practice, since the pk method is more expensive than the V-g method, it is only used when flight control systems are required to be modeled during the analysis.

In the characteristic determinant method the determinant value of the characteristic equation is determined with increasing frequency at constant altitude and velocity. The real parts of the determinant values are plotted against the imaginary parts. The way the results encircle the origin and the minimum distance to the origin for the involved resonant frequencies indicates the stability. This technique is also suitable to take into account the influence of flight control system.

The Nyquist method, known from control theory, is a comparable technique as the characteristic determinant method. The stability of the closed-loop system is determined using the so-called Nyquist criteria by inspecting the so-called Nyquist path, see standard books on control theory.

During flutter analysis, the unsteady aerodynamic forces associated with each mode shape are required for many combinations of k and Mach number. Furthermore, if the flight control system is considered aerodynamic forces associated with each control surface have to be calculated also. In practice, calculations are carried out for several conditions, and then, an interpolation method is applied to approximate the aerodynamic forces at the k-Mach plane. The interpolation method can be of spline type or Padé type method. When a Padé type method is used, the data to be interpolated can also be calculated from diverging motions ($\sigma \neq 0, \omega = 0$) instead of oscillatory motions ($\sigma = 0, \omega \neq 0$). This type of calculation offers many advantages compared to the traditional oscillatory motion, see [5, 7].

3.1 Linearized subsonic/supersonic method

When flow disturbance are small compared to the speed of sound and when thickness, angle of attack and slide slip angle decrease asymptotically with $|1 - M|$, the Kelvin-Bernoulli equation for the velocity potential may be used to represent the flow behavior. Following the input motion, the potential is assumed to have the form of (retaining only first order term):

$$\phi\langle \boldsymbol{x}, t\rangle = \phi_m\langle \boldsymbol{x}\rangle + \hat{\phi}\langle \boldsymbol{x}\rangle e^{st}. \tag{12}$$

Since the governing equation is linear two separate equations may be derived and employed independently for the mean part ϕ_m and the first harmonic $\hat{\phi}$ of the unsteady part. At NLR several methods have been developed for calculating the unsteady part using either pressure/acceleration potential (doublet-lattice method): VARDOB (subsonic), NLRI (subsonic including body effect) and GUL (subsonic/supersonic lifting surface) or directly using the velocity potential: CAR (subsonic/supersonic panel method).

3.2 Full-potential time-linearized method

Frequency domain techniques can still be applied to nonlinear equations, like full potential equation, through time-linearization. The dynamic state is assumed to be relatively small that the global behavior of the flow during the oscillation does not change, e.g. shock waves do not appear/disappear during part of the oscillation. Inserting equation (12) into the full-potential equation one obtains two equations for the mean condition and the first harmonic, respectively:

$$\mathcal{FP}\langle\phi_m\rangle = 0 \;\text{ and }\; \hat{\mathcal{FP}}\langle\phi_m;\hat{\phi}\rangle = 0, \tag{13}$$

where $\mathcal{FP}$ is a full potential operator. Note that the steady equation for ϕ_m is nonlinear and the time-linearized equation is linear for $\hat{\phi}$. Unlike the linear case, now the flow equation for the first harmonic depends on the solution of the steady equation which has to be solved first. A finite-volume/field panel method, called FTRAN3, is used to solve equation (13), see [6, 12] for detailed descriptions. It is generally known that solution methods for the time-linearized equation had long been plagued by a frequency limitation. A technique to relief this limitation is introduced by Hounjet and Eussen [7].

3.3 Frequency domain aerodynamic data from time-accurate CFD

Unsteady aerodynamic forces for oscillatory motion can also be obtained from a time-domain CFD method using the following techniques.

First, using identification of the CFD system by exciting it using a certain input signal and measuring the output response. The desired unsteady aerodynamic data are then obtained as*

$$L = \frac{\mathcal{FT}\langle\text{aerodynamic force response}\rangle}{\mathcal{FT}\langle\text{input motion}\rangle}, \tag{14}$$

*Note that the selection of amplitude of the motion is not trivial

where $\mathcal{FT}$ is a Fourier transform operator. For sinusoidal input signal, data for only one value of k can be obtained at a time, thus many flow simulations have to be carried out for various values of k. A more practical approach is to use impulse input signal which can give aerodynamic force data at a range of k for each flow simulation.

Second, using the harmonic constraint method introduced by Hounjet et al. [11]. In this method a sinusoidal input signal is assumed and the response is constrained to also a sinusoidal function while dropping the higher harmonics. Suppose that the airplane performs a sinusoidal motion in one of its modal modes at reduced frequency k. Let ϕ_0, ϕ_1 and ϕ_2 denote the current approximation to the solution at $t = 0, \Delta t$ and $2\Delta t$, respectively. Using the harmonic constraint:

$$\phi\langle t\rangle = \phi_m + a\cos kt + b\sin kt \tag{15}$$

a, b can be calculated from ϕ_1 and ϕ_2 which can then be used to update ϕ_0 and ϕ_{-1} (and ϕ_{-2} for a three-stage method). Next ϕ_1 and ϕ_2 are updated using the usual time-integration. The process is repeated until convergence is obtained. The unsteady aerodynamic force can be easily calculated from a and b. This scheme is called a 'two-step per cycle' technique. A typical convergence of the method can be seen in figure 2. This figure shows the iterates of the force components F_x and F_z and momentM_y for a NACA64A010 at transonic condition of M_∞=0.80 and k=0.20 for pitching oscillation about half chord. When diverging motion is used, the solution is constrained as:

$$\phi\langle t\rangle = \phi_m + ae^{pt}, \tag{16}$$

where $p = \sigma L/V$. Only ϕ_1 needs to be calculated using the time integration method and the scheme is called 'one-step per cycle' technique.

4 Computational Aeroelastic Simulation

The general approach follows the loosely-coupled scheme in which methods are employed to solve the structural and flow equations separately with certain fluid-structure coupling conditions (in space and in time) at the fluid-structure interface. This technique would benefit from the matured methods which have been developed for each field.

The complete set of equations of motion, equation (4) is reduced to a first order system as:

$$\begin{Bmatrix} \dot{q} \\ \dot{\dot{q}} \end{Bmatrix} = \begin{bmatrix} I & 0 \\ M^{-1}K & M^{-1}C \end{bmatrix} \begin{Bmatrix} q \\ \dot{q} \end{Bmatrix} + q_\infty S \begin{bmatrix} 0 \\ M^{-1} \end{bmatrix} \{Q\} \ , \tag{17}$$

which can be recast into:

$$\{\dot{\boldsymbol{x}}\} = \left[\overline{A}\right] \{\boldsymbol{x}\} + q_\infty \left[\overline{B}\right] \{\boldsymbol{u}\} , \tag{18}$$

where $\overline{A}$ and $\overline{B}$ are constant matrices that result from the change of the variables $\boldsymbol{x} = [q, \dot{q}]^T$ and $\boldsymbol{u}$ is the coefficient of generalized aerodynamic force $Q\langle q, \dot{q}\rangle$. The aeroelastic time-marching solution procedure applied to integrating equation (18) employs transfer matrix methods [3, 21] or the Newmark method [8].

4.1 Full-Potential flow modeling

The CAS system using full-potential flow method called AESIM [8] is developed with the objective to assist in the design of future aircraft which are subjected to increases in flexibility, aerodynamic loading and nonlinearity; this system can be of value in the early design and development phase for assessing flight stability and control, safety and risk evaluation and ride qualities. The method focuses primarily on aeroelasticity at transonic and low supersonic flow conditions near Mach=1 where aerodynamic nonlinearities are a non-negligible factor and the accuracy of conventional methods is most uncertain. AESIM consists of the FOLDIT/BLOWUP structured monoblock grid generator, the NASAES elastomechanical data manipulation and AESIM-core.

Main features of AESIM include: interactive or macro mode, quick turn around time thanks to advanced solution methods, extensive options of type and method of analysis, see [8, 11] for more detailed descriptions of the method. AESIM has currently matured to the level of industrial

applications.

4.2 Euler/Navier-Stokes flow modeling

Current developments at NLR are aimed at a general fluid-structure interaction model and are concentrated on the flow modeling because applications for military aircraft at off-design condition and more complex configurations are desired. Work is underway to implement an interaction scheme in the NLR structured-multiblock Euler/Navier-Stokes method [1], ENFLOW system, for aeroelastic simulation purposes. The block diagram of the fluid-structure interaction scheme is shown in figure 3. ENFLOW consists of domain modeler ENDOMO, grid generator ENGRID, flow solver ENSOLV and grid adaptor ENADAP and has been used extensively at the NLR for variety of complex flow problems including: determination of aerodynamic forces on aircraft, engine nacelle (power on/off) analysis, supersonic missile, oscillating wing, buffet, etc.

One of the important components is the development of a multiblock deforming grid capability. Current approaches available from the literature mostly use a set of equations for the coordinates and solve it at each time step (e.g. spring system, Laplace, etc.). Here, a different approach is taken, in which similar building blocks as the interpolation method for the transfer of the displacement data from the structural nodes into the aerodynamic control-points are employed to extrapolate the displacement on the aerodynamic surface grid into the grid on the field. This means that a real three-dimensional interpolation method has to be used for which the volume spline method of Hounjet and Meijer [10] is most suitable. The core of the volume-spline function of Refs. [10] is slightly modified to account for zero deformation at the outer boundary of the aerodynamic grid. The spline matrix has to be generated only once, i.e. before the flow simulation is carried out. In other words the governing equations for the grid deformation is solved once instead of at each time step like the common method. In practice, the volume spline is applied only for the block boundary and the grid inside each block is deformed using a transfinite interpolation. The grid deformation can be done completely independently for each block which preserves the block-wise parallelization scheme of ENSOLV.

4.3 Nonlinear semi-empirical model

For aeroelastic analysis of nonlinear limit cycle oscillations aeroelastic simulations are required over a large number of periods. As a first approach a semi-empirical model has been developed by Meijer [16], Meijer and Cunningham, Jr. [18] to understand LCO phenomena and enable routine applications.

In this model the most important phenomena which influence the nonlinear airloads are repre-

sented in a set of ordinary differential equations and subsequently the coefficients are fitted to experimental data for certain conditions. Assuming the generality of the model it is then applied to a wider range of conditions.

The NLR semi-empirical model is based on the ONERA model usually used for dynamic stall modeling of helicopter blades, see Peters [19], Petot and Dat [20]. The basic principles and equations used in the model are illustrated in figure 4. The three equations shown in figure 4 are the generalized differential equations necessary to establish a nonlinear relationship between $C_F(\tau)$ and the displacement variable q (which is typically angle-of-attack, α). The functions and coefficients have been designed by Petot and Dat [20] to give the Theodorsen solution in the case of a flat plate in a perfect flow.

The first equation in ONERA model simply states that the nonlinear function $C_F(\tau)$ is the sum of a linear part, $C_{F_1}(\tau)$, and a nonlinear part, $C_{F_2}(\tau)$. $C_{F_1}(\tau)$ is defined by the linear part of the $C_{F_s} \equiv C_{F\,\mathsf{lin}}$ curve (figure 4). The determination of $C_{F_1}(\tau)$, containing circulatory and noncirculatory parts (see [20]), is obtained through the satisfaction of the conditions posed by the second equation. This equation, when used in the linear region, provides a full accounting of the unsteady aerodynamic effects including time lag and flow inertia effects. These effects are analogous to the Theodorsen function in two dimensional oscillatory aerodynamics.

$C_{F_2}(\tau)$ has to be determined when the characteristics depart from the linear variation $C_{F\,\mathsf{lin}}$ using the third equation which is a damped-mass-spring system forced by nonlinear function. The unknown a_2 and a_3 parameters represent a "damping" and "stiffness" (or "frequency") respectively for the equivalent spring-mass system.

The parameters a_1, a_2, a_3 and functions f_1 and f_2 are assessed using experimental data for a relevant configuration or from flow simulation using CFD, see [18] for a more detailed description.

The basic principles of NLR unsteady pressure model, shown in figure 5 are essentially the same as those for the ONERA model, but now applied to the individual pressures over the wing area. The nonlinear variation of $C_p(\tau)$ is the sum of two parts $C_{p_1}(\tau)$ and $C_{p_2}(\tau)$, where the former is primarily governed by the slope of $C_{p\,\mathsf{lin}}$ and the latter by ΔC_{p_s}, the difference of C_{p_s} and $C_{p\,\mathsf{lin}}$. In the same way as for the ONERA model the position of $C_{p\,\mathsf{lin}}$ was determined originally by the linear variation of C_{p_s} with α for conditions of attached flow (small incidences) where no changes occur in flow fields such as shock passages and shock-induced and trailing-edge separation as illustrated in figure 5. However, taking into account correctly the local nonlinear features of flow

fields such as shock passages, etc. at higher incidences, the meaning of $C_{p\,\mathrm{lin}}$, ΔC_{p_s} and their derivatives has been redefined in the NLR pressure model. This modified approach consists of locally developed $C_{p\,\mathrm{lin}}$ and ΔC_{p_s} with α. So, the main difference with the ONERA model is that the complete set of equations is applied at each event, i.e. no distinction is made between linear and nonlinear portions of the C_{p_s} curves. This implies that all unknown parameters (a_1, a_2 and a_3, and five parameters in the functions f_1 and f_2) have to be determined a priori for each reference angle-of-attack α_r and each pressure location at a given Mach number.

The instantaneous differential pressure distribution on the wing can then be calculated using the data of local angle of attack distribution:

$$\alpha = \alpha_m + \Delta\alpha, \tag{19}$$

$$\alpha_m = \alpha_p + \frac{\partial}{\partial x} h_m, \tag{20}$$

$$\Delta\alpha = \sum_{N_R+N_E} \left(\frac{\partial}{\partial x} + \frac{1}{V}\frac{\partial}{\partial t} \right) \phi_j q_j \langle t \rangle. \tag{21}$$

α_p is the prescribed angle-of-attack, and $\Delta\alpha$ the time-dependent variation at a certain point.

4.4 MIMO-class system identification

One of the problems in aeroelastic simulation technology which has hardly been addressed in the literature is the post-processing of the time trace results to obtain the flutter point. The common method is to carry out simulations for a number of dynamic pressures covering stable and unstable conditions. Subsequently the damping is extracted from each simulation and interpolated to the value of zero.

In the current development at NLR a more efficient approach is sought with the so-called multi input/multi output technique. The adoption of MIMO [4] technology permits a black box evaluation of the aeroelastic system in such a way that after a single fully-coupled simulation for one flight condition the system state for other flight conditions (e.g. q_∞) may be predicted. MIMO also permits the extraction of useful data (e.g. generalized forces) from the coupled simulation which can be used for other purposes.

The essence of the method to identify the aeroelastic system by fitting the time trace to a certain

MIMO model of the aeroelastic system. An important requirement is that all the related modes should be excited for completeness of the resulting model. More detailed discussions concerning the possibility to identify the system in frequency or time domain may be found in Ref.[9].

Two schemes are introduced in Ref. [4], i.e. decoupled and coupled technique. The first technique is used here. This technique can be explained better using a discrete-time linear system. After a certain approximation to equation (18), e.g. using Newmark or transition matrix method [21], the discrete state space equation is obtained as:

$$\{\boldsymbol{x}\}_{k+1} = \left[\hat{A}\right]\{\boldsymbol{x}\}_k + q_\infty \left[\hat{B}\right]\{\boldsymbol{u}\}_k, \tag{22}$$

where subscript k represent an evaluation at a discrete time t_k. The coefficient of the generalized force is approximated using a linear function of the state variable as:

$$\{\boldsymbol{u}_k\} \approx [\mathcal{U}_0]\{\boldsymbol{x}_k\} + [\mathcal{U}_{-1}]\{\boldsymbol{x}_{k-1}\} + ... + [\mathcal{U}_{-N}]\{\boldsymbol{x}_{k-N}\}, \tag{23}$$

where N is called the order of the model; note that $\boldsymbol{u}$=0 for the mean displacements h_m. The coefficients of the approximation can be obtained using a least square regression applied to the pair of $\boldsymbol{u}_k$ and $\boldsymbol{x}_k$ data resulting from an aeroelastic simulation. Without loosing the generality a first order model is used. Introducing a new state vector $\{\boldsymbol{y}\}$ and the transformation

$$\left\{ \begin{array}{c} \boldsymbol{y}_1 \\ \boldsymbol{y}_2 \end{array} \right\}_k = \left\{ \begin{array}{c} \boldsymbol{x}_k \\ \boldsymbol{x}_{k+1} \end{array} \right\}$$

and inserting equation (23) the discrete state equation for the whole aeroelastic system becomes:

$$\{\boldsymbol{y}\}_{k+1} = \left[\hat{A}'\right]\{\boldsymbol{y}\}_k, \tag{24}$$

where the new system dynamic matrix is

$$\left[\hat{A}'\right] = \left[\begin{array}{cc} 0 & I \\ q_\infty[\hat{B}][\mathcal{U}_{-1}] & [\hat{A}] + q_\infty[\hat{B}][\mathcal{U}_0] \end{array} \right] \tag{25}$$

The stability of a system represented by a discrete state space equation (24) may be inspected from the eigenvalues of $[\hat{A}']$ which depend on the parameter q_∞. The flutter boundary is the value of q_∞ at which one of the eigenvalues reaches a unit value. For more detailed description of the method Ref. [4] should be consulted.

5 Applications

To demonstrate the applicability of the aeroelastic methods, a typical example of flutter clearance is presented. The selected example is an air-to-ground F-16 configuration as defined in figure 6; the configuration is symmetric and includes:

- fuselage fuel tank,
- wing fuel tank,
- centerline pod,
- 370 USG fuel tank at wing station BL71,
- VER-4 rack at wing station BL120,
- missiles at wing stations BL157 and BL180.

The type of weapons carried on the VER-4 racks belongs to the class of 500 to 600 lbs stores.

The structural model of the F-16 aircraft, made available to NLR by GENERAL-DYNAMICS, is shown in figure 7. The model consists of a condensed finite element model supplemented by modules of finite element models of the various cantilever pylon/store(s) combinations. The unsteady aerodynamic model uses either VARDOB, NLRI or GUL for subsonic flow and CAR or GUL for supersonic flow. The aerodynamic paneling of the surface is shown in figure 8. Since VARDOB and GUL can not model thick bodies, the fuselage is represented by an open cylinder in order to maintain the correct aerodynamic interference. Except for the tip launcher and/or missiles, the representation of wing stores is omitted in the aerodynamic model. NLR studies concerning wing stores have made it plausible that the effects of the underwing stores on the unsteady components of the aerodynamic forces are small. The aerodynamic influence of the tip launcher with or without tip missile, however, can be considerable.

Examples of calculated flutter results are presented in figures 9 and 10. Figure 9 shows results of the fully loaded VER-4 racks (configuration A). The mechanism of the antisymmetric flutter instability is governed by two vibration modes: wing torsion (mode 1) and tip missile pitch (mode 3). The calculated flutter speed, however, is well beyond the operational speed limit (about 600 KEAS). However, when two stores are left out from the VER-4 rack, either inboard or outboard, a serious instability appears at about 400 KEAS within the operational speed regime, as shown in figure 10 (configuration B). The same flutter mechanism is acting there, involving the wing torsion (mode 1) and the tip missile pitch (mode 2); the two interacting modes are shown in figure 11.

As the flutter predictions for VER-4 configuration are obtained with linear subsonic and supersonic unsteady aerodynamics, the accuracy of the predictions in the transonic speed range remains uncertain especially when flow separation occurs. When the flow is still attached the linear method performs quite well compared to the transonic method at least to determine the boundary of instability, see figure 12. This negligible effect on the flutter boundary is perhaps due to the fairly high frequency at which flutter occurs.

The condition beyond the flutter boundary is also of interest because extensive flight test programs [14] revealed instabilities of LCO type at transonic conditions, especially with the configurations: VER-4 with two stores installed and with tip missiles (configuration B) and VER-4 without wing stores and without missiles. The NLR-method for LCO prediction using the semi-empirical model is therefore applied. In the early model [14], only steady wind-tunnel data are used. This approach has been found useful to indicate the occurrence of LCO for a certain configuration.

Results using an early version of the NLR-model for F-16 configurations with VER-4 and a number of its downloadings, D.1 to D.4 are presented in figure 13. For each downloading case two fuel states are inspected: full tank (configuration a) and empty tank (configuration b). The analysis has been carried out for the flight conditions of Mach number 0.92 and altitude 5K ft. The structural modal damping is assumed to be 1%, i.e. g= 0.01. For each configuration shown in figure 13 natural modes up to 15 Hz are included in the analysis which lead to the number of DOF between 16 and 20. The calculations are carried out over 30 seconds (about 450 periods of the highest mode), while the angle of attack changed linearly from 1 to 10 deg. Prior to time-domain simulations, the classical flutter analysis is carried out using V-g method.

	linear analysis	nonlinear analysis
D.1a	severe flutter at 5 Hz	LCO at 5 Hz
D.1b	–	–
D.2a	–	–
D.2b	–	–
D.3a	–	–
D.3b	lowly damped mode at 7.5 Hz	LCO-sensitive at 7.5 Hz
D.4a	mild flutter at 11.5 Hz	LCO-sensitive at 11.5 Hz
D.4b	–	–

Table 1 Summary of classical linear and semi-empirical nonlinear analyses of VER-4 downloadings D.1 to D.4; fuel state 'a' designates a full tank and fuel state 'b' designates an empty tank

The results of classical linear and nonlinear LCO simulations are summarized in figure 13 and table 1. Maximum response levels are predicted at about mean angles of attack of 6 and 2 deg. Repeating the LCO calculations for downloading D.1 and constant mean angle of attack of 6 deg yielded the following acceleration levels: acc.1: 16.0g, acc.2: 6.3g and acc.3: 1.6g. Available flight test data for these configurations correlate qualitatively quite well with the calculated responses. However, the predicted level of acceleration is too high compared to the level experienced during the flight test. Artificial damping, which is case-dependent, has to be added to have a correct acceleration level.

This deficiency of the early version motivated further development of the NLR model to arrive at the NLR pressure model described in section 4.3. The model benefits also from the unsteady flow measurement data. The model has been successfully applied for wider range of heavy-store configurations giving a correct acceleration level, see Ref. [17]. The summary of the acceleration levels obtained using the NLR pressure model are shown in figure 14. Three configurations differing only at the mid station, i.e. BL120, are presented:

– Configuration C: various types of a single-heavy-store at BL120,
– Configuration D: TER-9 store rack at BL120,
– Configuration E: VER-4 store rack at BL120.

At other stations, the same stores are installed as the case described in the previous paragraph. Store configurations C.1 to C.5 differ in their mass. The acceleration levels shown in figure 14 correlate quite well to the one observed during flight testing in wind-up turn maneuver.

The preliminary results of the aeroelastic simulation using ENFLOW system are now presented. The structural model is the standard AGARD aeroelastic configuration of weakened wing number 3 of 445.6 [22]. Figure 15 shows the example of the results of the multiblock grid deformation technique where the wing surface is artificially deformed using the second bending mode.

For the aeroelastic simulation the Euler mode of ENSOLV is used. Since very small displacements are expected to occur, the transpiration boundary condition is applied on the surface. The first two modes of the wing 445.6 are employed to model the structural dynamics part. These modes should interact to produce a classical bending-torsion type flutter [2, 8, 13, 21, 22]. Lee-Rausch and Batina [13] show that the effect of the inclusion of more modes is minor. For the simulation an initial condition of $\dot{q} = 0.0001$ is applied to all modes. Figure 16 shows the response of the first and second mode expressed in the generalized coordinates at various dynamic pressures characterized by the speed index, V^* defined here as $V_\infty / (\omega_2 b_r \sqrt{\mu})$, where b_r is the half of the root-chord,

μ is the mass ratio and ω_2 is the circular frequency of the second mode. The time on the x-axis is nondimensionalized by the wind-off period of the second mode. Figure 17 presents the generalized forces corresponding to the first and second mode. By inspecting the period of the responses, it can be seen from figures 16 and 17 that at the beginning of the simulation the contribution of the second mode is present and is quickly damped while the first mode has very small damping. This is the common situation close to flutter. Stable (V^*=0.275), neutral (V^*=0.287) and slightly unstable (V^*=0.300) responses are obtained. After the simulations, the damping of the response is extracted using a simple logarithmic-decrement technique and interpolated to the value of zero at which the flutter speed index is obtained. The comparison with available data in the literature is shown in table 2.

Method		V_f^*
Experiment [22]		0.3076
CFL3D [13]	(Euler)	0.256
	(Navier-Stokes)	0.287
Ref. [2]	(Euler)	0.300
AESIM	(Full-Potential)	0.303
ENFLOW	(Euler)	0.291

Table 2 Comparison of flutter point at M_∞=0.96 for AGARD standard test case of 445.6 wing

Example of the applications of MIMO technique to identify the coupled aeroelastic system is shown in figures 18 and 19. Two aeroelastic simulations have been carried out for subcritical and supercritical conditions at M_∞=0.901. Subsequently, the MIMO model is fitted to the time trace of the subcritical condition, the results are shown in figure 18. The extracted MIMO model is then used to predict the situation at the supercritical dynamic pressure. In figure 19 the predicted time traces are compared with the real aeroelastic simulation. It can be seen that the MIMO model prediction performs very well for the lower 3 modes. The amplitude of mode 4 (second torsion mode) is overpredicted.

6 Concluding Remarks

In this paper an overview has been presented concerning the current capability at NLR in predicting flutter characteristics for clearance purposes. Current capabilities have been developed in a cooperation with The Royal Netherlands Air Force. Present developments at NLR and some preliminary results have also been presented.

In a flutter clearance process the classical linear methods play an important role. Nonlinear methods are applied only for ambiguous conditions or beyond the flutter boundary. Therefore part of current NLR activities is to continue the support of potential-flow methods, and to extend the potential-flow based aeroelastic models to include a coupling with flight control systems, to enable the analysis of aeroservoelastic problems.

The other front concerns the prediction of the aeroelastic behavior of complex configurations involving turbulent vortex flows, shock-induced separations and large structural deformation. On this front the time-domain approach is adopted in combination with a general fluid-structure coupling and the Euler/Reynolds-Averaged Navier-Stokes equations to develop new aeroelastic analysis capability.

Bibliography

1. J.W. Boerstoel. ENFLOW a system of CFD codes for industrial CFD analysis of flows around aircraft including propulsion systems modelling. NLR CR 93519, NLR, 1993.
2. C. Farhat and M. Lesoinne. Fast staggered algorithms for the solution of three-dimensional nonlinear aeroelastic problems. In *Numerical Unsteady Aerodynamics and Aeroelastic Simulation*, AGARD Report R-822, pp 7–1∼7–11, 1998.
3. J.W. Edwards, R.W. Bennett, W. Whitlow Jr, and D.A. Seidel. Time marching transonic flutter solutions including angle of attack effects. AIAA Paper 82-0685, AIAA, 1982.
4. B.J.G. Eussen, M.H.L. Hounjet, and M.W. Soijer. Comprehensive Time Analysis in Aeroelastic Simulations. In *Proceedings of 21st Congress of ICAS*, ICAS 98-2.6.3, Melbourne, 1998. International Council of the Aeronautical Sciences, AIAA Electronic Publications.
5. M.H.L. Hounjet. Application of diverging motions to calculate loads for oscillating motions. *AIAA Journal*, Vol. 24, No. 10, pp 1723–1725, 1986.
6. M.H.L. Hounjet. FTRAN3S and FTRAN3: Methods to calculate steady and time linearized unsteady transonic flows about wings. Technical Report TR 87020, NLR, 1987.
7. M.H.L. Hounjet and B.J.G. Eussen. Beyond the frequency limit of time-linearized methods. NLR Report TP-91216, NLR, 1991.
8. M.H.L. Hounjet and B.J.G. Eussen. Outline and application of the NLR aeroelastic simulation method. In *Proceedings of 19th Congress of ICAS*, pp 1418–1441, Anaheim, 1994. ICAS, also NLR-TP-94422, NLR, 1994.
9. M.H.L. Hounjet, B.J.G. Eussen, and M. Soijer. Analysis of aeroelastic simulations by fitting time signals. In *Proceedings of 1997 CEAS International Forum on Aeroelasticity and Structural Dynamics*, volume 3, pp 131–141, Rome, 1997. Associazione Italiana di Aeronautica ed Astronautica, also NLR-TP-97281, NLR, 1997.
10. M.H.L. Hounjet and J.J. Meijer. Evaluation of Elastomechanical and Aerodynamic Data Transfer Methods for Non-planar Configurations in Computational Aeroelastic Analysis. In *Proceedings of 1995 CEAS International Forum on Aeroelasticity and Structural Dynamics*, pp 11.1–11.24, Manchester, 1995. Royal Aeronautical Society, also NLR-TP-95690, NLR, 1995.
11. M.H.L. Hounjet, B.B. Prananta, and B.J.G. Eussen. Frequency domain unsteady aerodynamics in/from aeroelastic simulation. In *Proceedings of 1999 International Forum on Aeroelasticity and Structural Dynamics*, Williamsburg, 1999. CEAS/AIAA/ICASE/NASA Langley, also NLR-TP-99256, NLR, 1999.
12. M.H.L. Hounjet, J.Th. van der Kolk, and J.J. Meijer. Application of NLR's calculation methods to transonic flow about oscillating wings. *AIAA Journal*, Vol. 22, No. 12, pp 1034–1042, 1985.

13. E.M. Lee-Rausch and J.T. Batina. Calculation of AGARD wing 445.6 flutter using Navier-Stokes aerodynamics. AIAA Paper 93-3476-CP, AIAA, 1993.
14. J.J. Meijer. NLR investigations to the flutter certification of aircraft with external stores. In *17th Annual Symposium of the Society of Flight Test Engineers*, Washington, D.C, 1986. Society of Flight Test Engineers, also NLR-MP-86025, NLR, 1986.
15. J.J. Meijer. NLR investigations of flutter behaviour of fighter aircraft with external stores. Report NLR-TP-91134, NLR, 1991.
16. J.J. Meijer. Determination of transonic unsteady aerodynamics loads to predict the aeroelastic stability of fighter aircraft. In *Proceedings of 1997 CEAS International Forum on Aeroelasticity and Structural Dynamics*, volume 2, pp 373–382, Rome, 1997. Associazione Italiana di Aeronautica ed Astronautica, also NLR-TP-97304, NLR, 1997.
17. J.J. Meijer and A.M. Cunningham Jr. Outline and applications of a semi-empirical method for predicting transonic limit cycle oscillation characteristics of fighter aircraft. In *Proceedings of 1995 CEAS International Forum on Aeroelasticity and Structural Dynamics*, pp 1–21, Manchester, 1995. Royal Aeronautical Society, also NLR-TP-95308, NLR, 1995.
18. J.J. Meijer and A.M. Cunningham, Jr. A semi-empirical unsteady nonlinear aerodynamic model to predict transonic LCO characteristics of fighter aircraft. AIAA Paper 95-1340, AIAA, 1995, also NLR-TP-95183, NLR, 1995.
19. D.A. Peters. Toward a unified lift model for use on rotor blade stability analysis. In *40th Annual National Forum on the American Helicopter Society*, Arlington, VA, 1984. American Helicopter Society.
20. D. Petot and R. Dat. Unsteady aerodynamic loads on an oscillating airfoil with unsteady stall. In *2nd Workshop on Dynamics and Aeroelasticity Stability Modeling of Rotorcraft Systems*, Boca Raton, 1987. Florida Atlantic University.
21. B.B. Prananta and M.H.L. Hounjet. Large time step aero-structural coupling procedures for aeroelastic simulation. In *Proceedings of 1997 CEAS International Forum on Aeroelasticity and Structural Dynamics*, volume 2, pp 63–71, Rome, 1997. Associazione Italiana di Aeronautica ed Astronautica, also NLR-TP-97619, NLR, 1997.
22. E.C. Yates Jr. AGARD standard aeroelastic configurations for dynamic reponse, I-wing 445.6. Report R-765, AGARD, 1988.

Figures

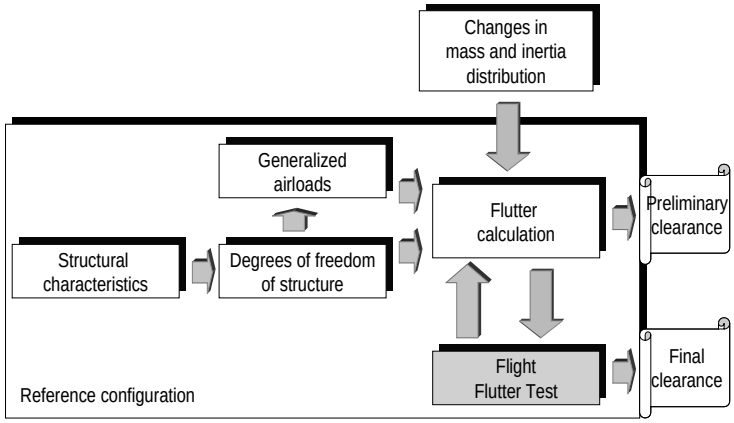

Fig. 1 NLR flutter clearance procedure for aircraft with stores

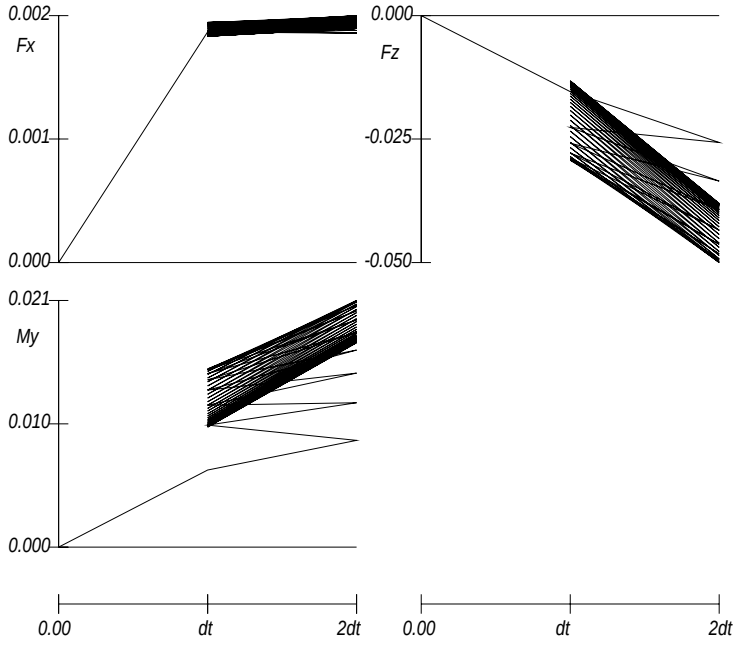

Fig. 2 Iterates of force components F_x and F_z and moment M_y during "2-step per cycle" iterations of harmonic constraint method, NACA64A010 *at M_∞=0.80, k=0.20 in pitching mode; 36 cycles are shown*

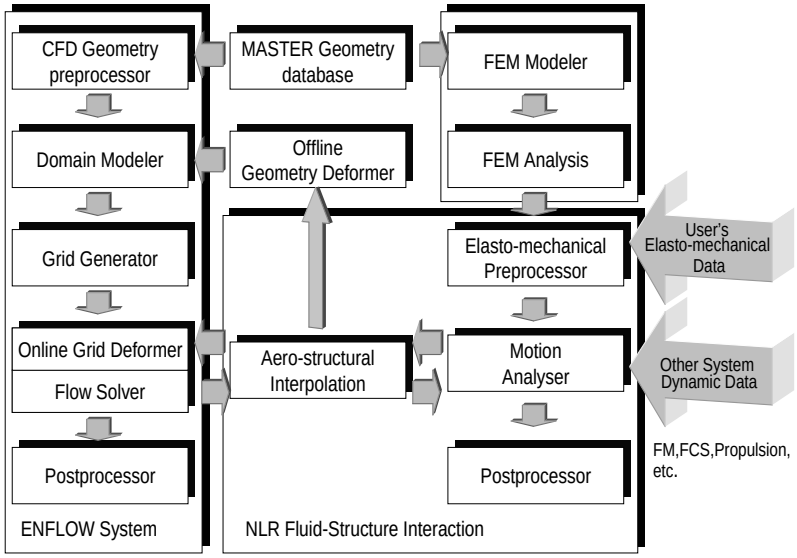

Fig. 3 Block diagram of NLR *fluid-structure interaction model*

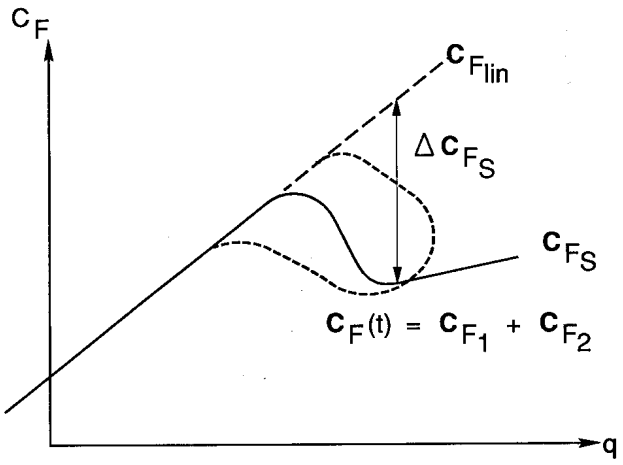

$$C_F = C_{F_1} + C_{F_2}$$

$$\dot{C}_{F_1} + a_1 C_{F_1} = f_1(q, \dot{q}, \ddot{q})$$

$$\ddot{C}_{F_2} + a_2 \dot{C}_{F_2} + a_3 C_{F_2} = f_2(q, \dot{q}, \ddot{q}, \Delta C_{F_S})$$

Fig. 4 Generalized ONERA *semi-empirical model*

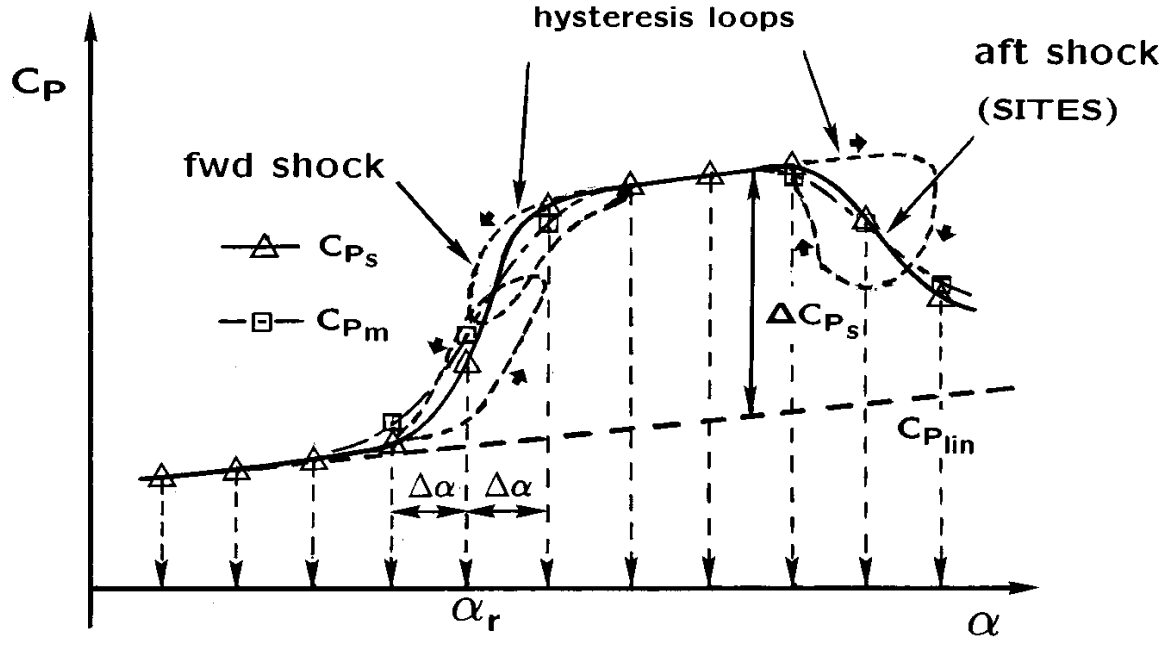

Fig. 5 NLR *unsteady pressure semi-empirical model (*SITES=*Shock-Induced Trailing-Edge Separation)*

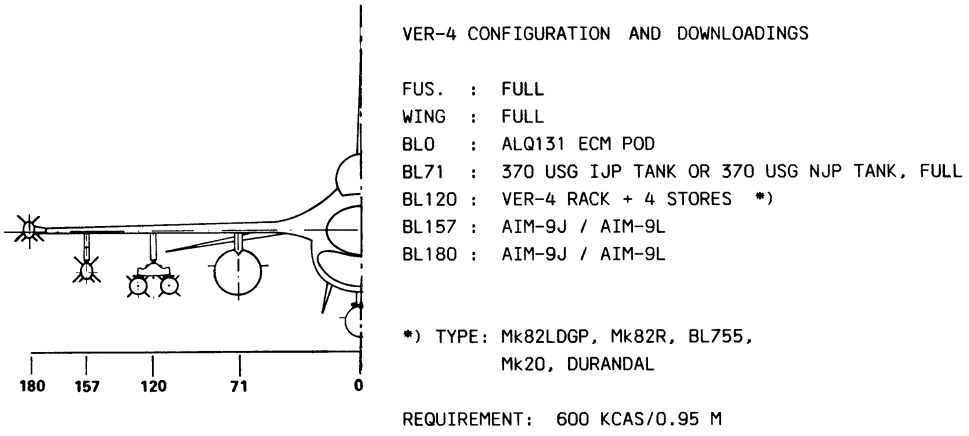

Fig. 6 F-16 *configuration with* VER-4 *multi-store racks*

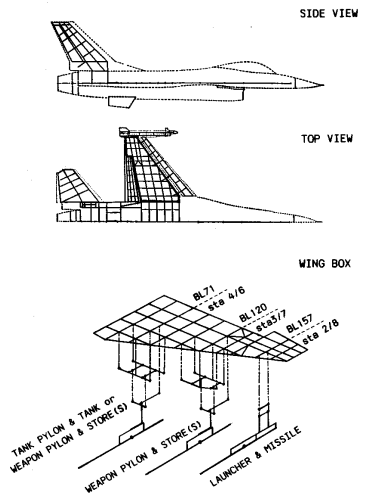

Fig. 7 F-16 structural representation and pylon/structure attachments to wing box (General Dynamics)

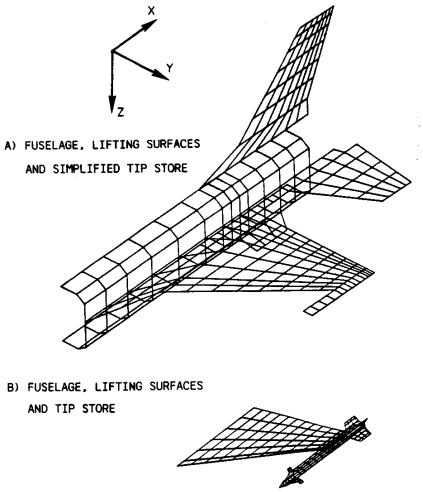

Fig. 8 F-16 unsteady aerodynamic paneling

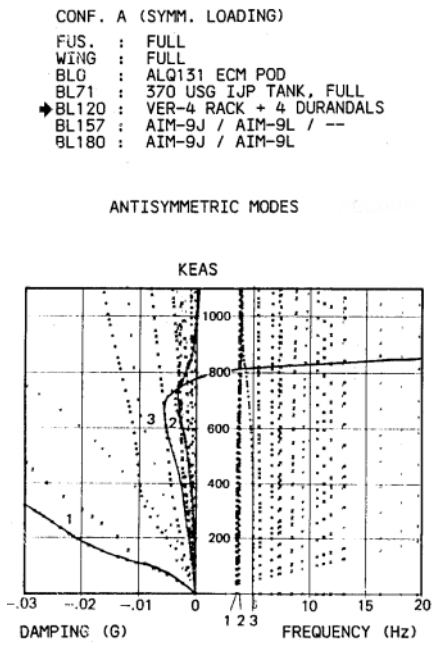

Fig. 9 Flutter characteristic of A configuration showing influence of the loading at BL120

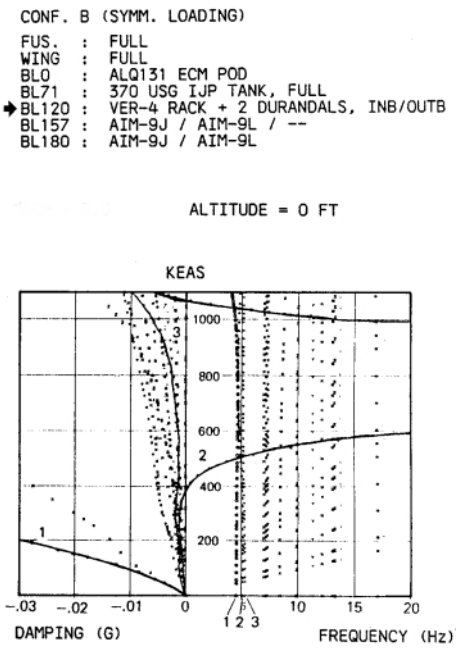

Fig. 10 Flutter characteristic of B configuration showing influence of the loading at BL120

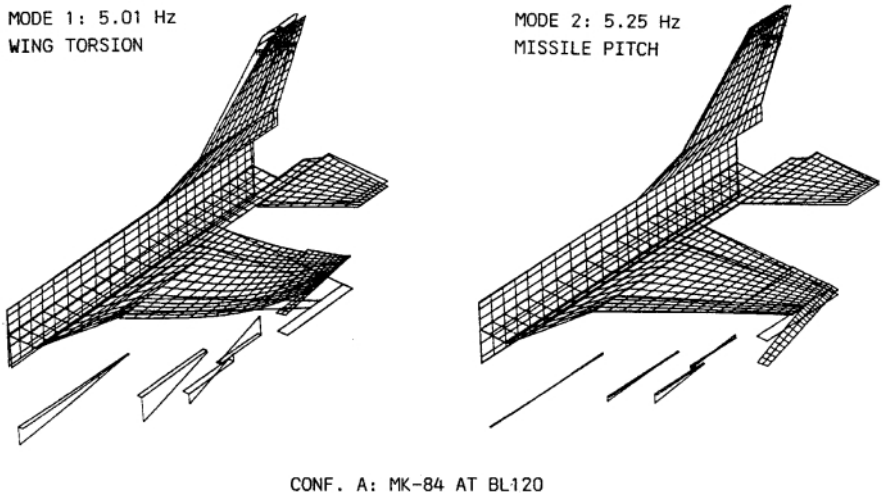

Fig. 11 Two interacting modes, wing-torsion and missile pitching, governing the flutter mechanism of F-16

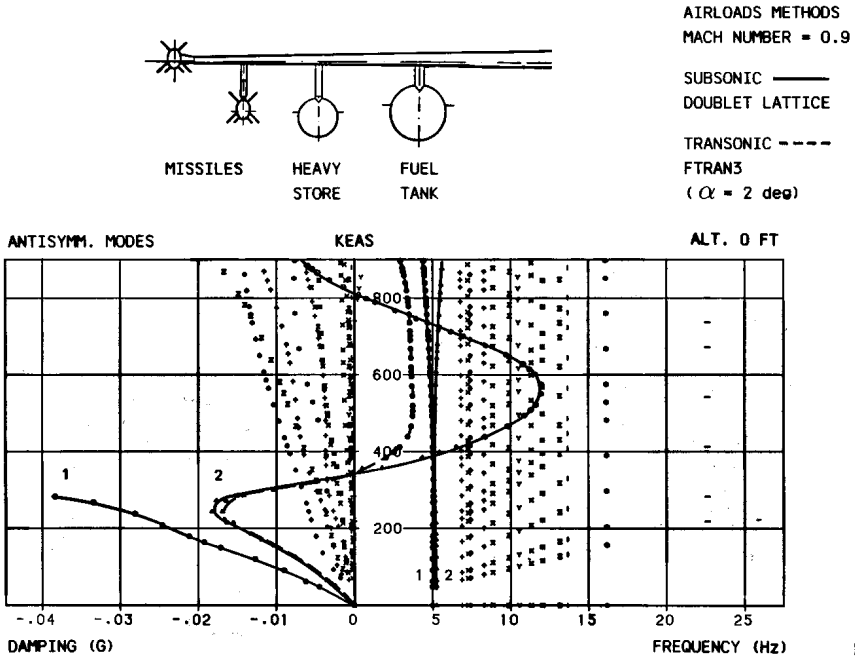

Fig. 12 Influence of transonic airload versus subsonic airload on calculated flutter characteristics

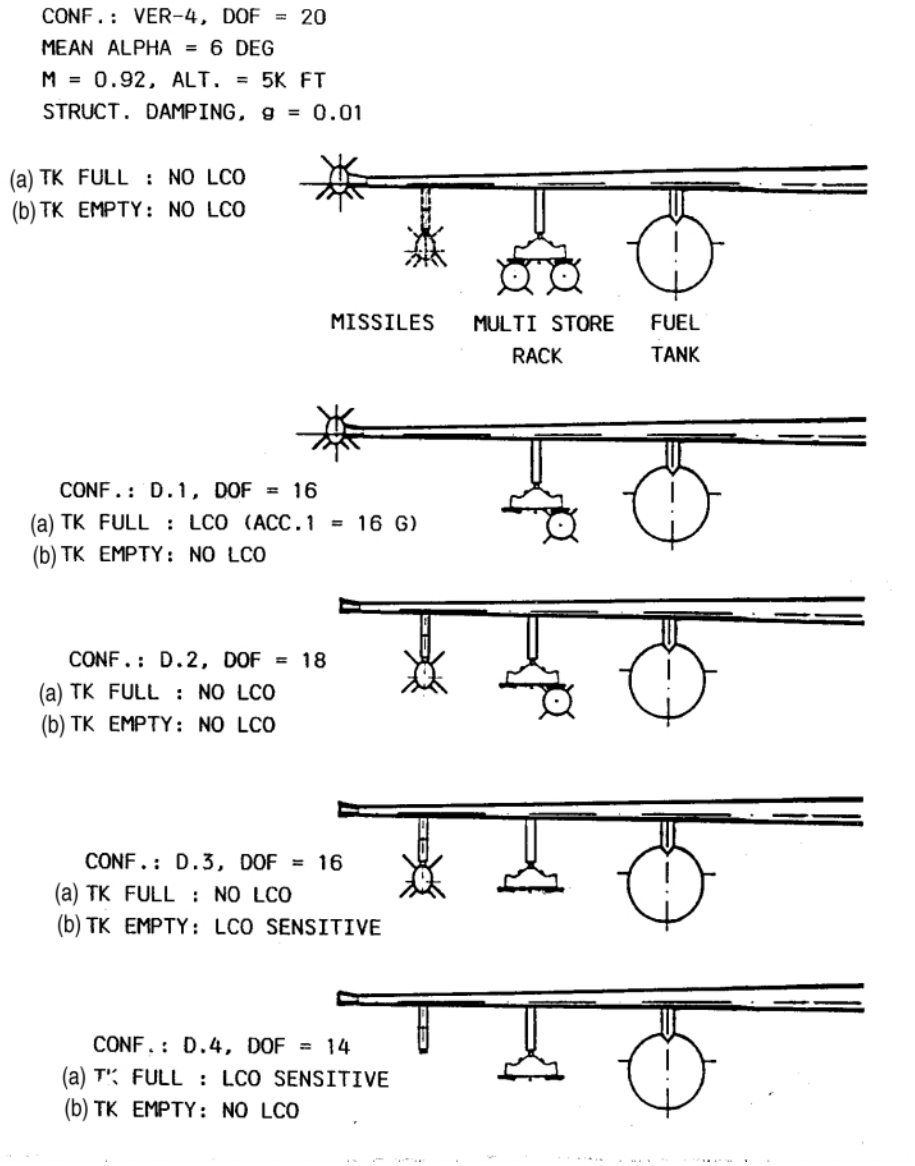

Fig. 13 Summary of LCO *investigation using early* NLR *model for* F-16 *equipped with* VER-4 *multi-store racks and downloadings; M=0.92, altitude = 5K ft*

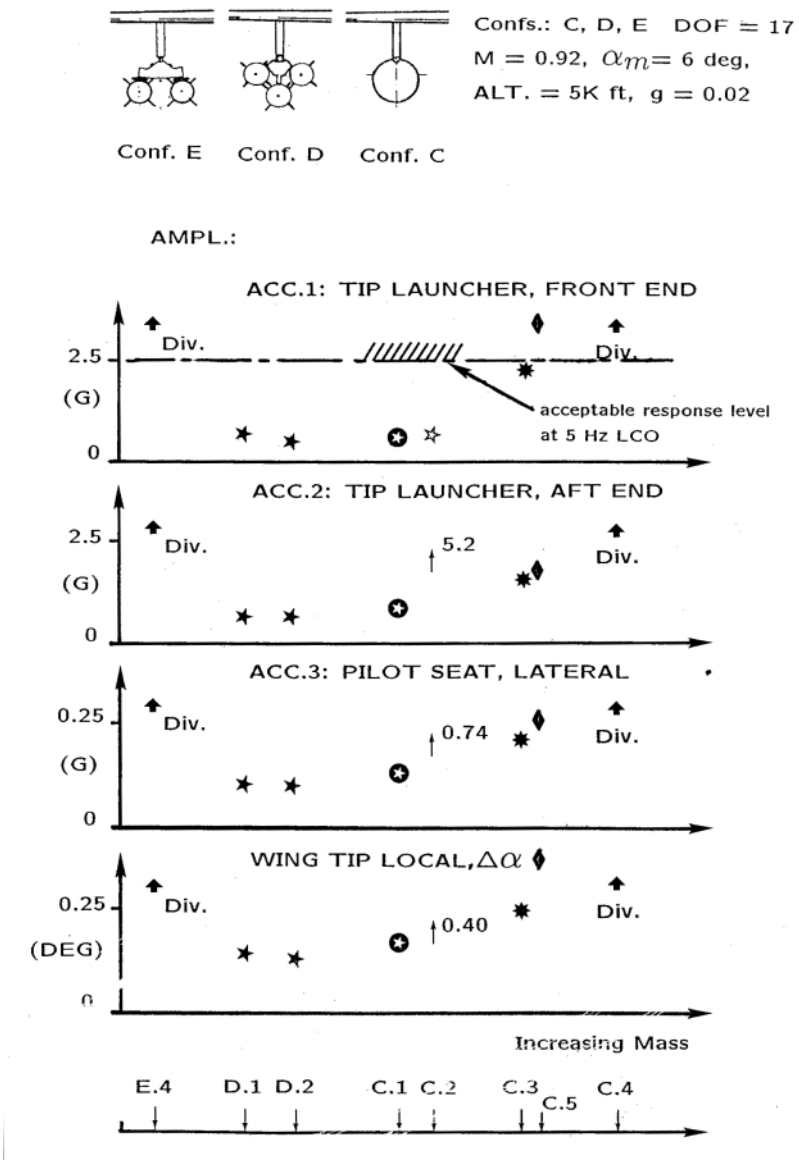

Fig. 14 Calculated dynamic loads during LCO *of* F-16 *configurations equipped with various heavy-store at wing station* BL120*: (C) a single heavy store, (D)* TER-9 *multi-store rack and (E)* VER-4 *multi-store rack, ordered in terms of mass; M=0.92, altitude = 5K ft*

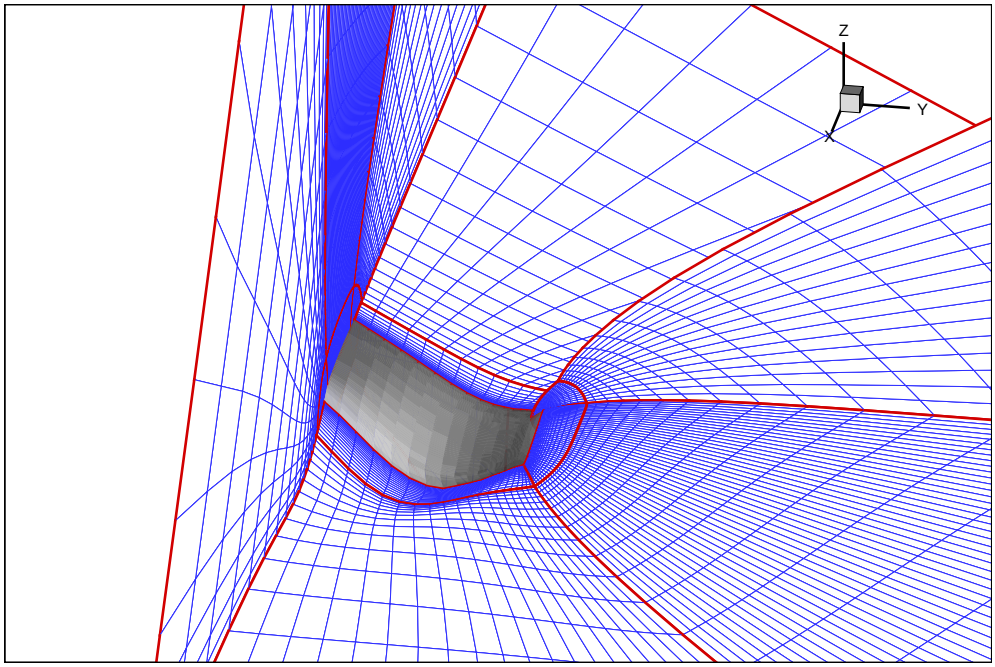

Fig. 15 Deformed multiblock grid about AGARD 445.6 *wing due to second bending mode*

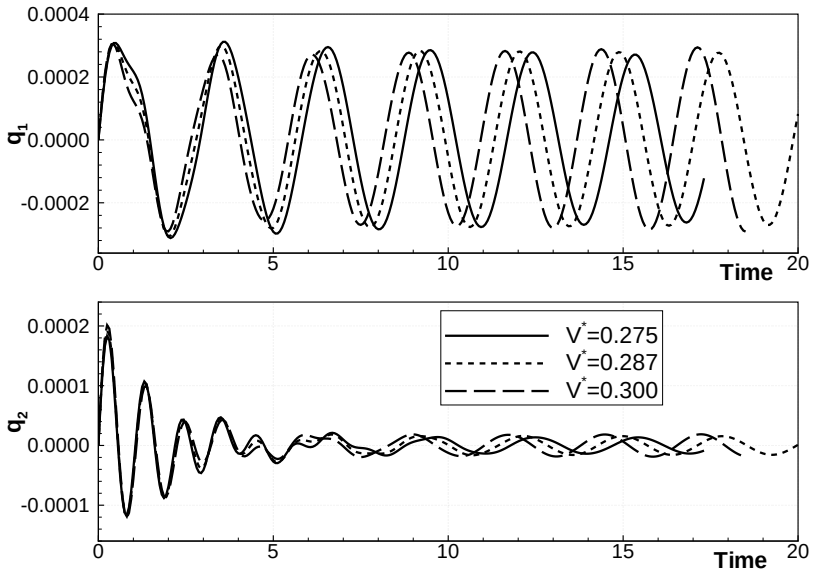

Fig. 16 Generalized coordinate of the first and second mode at three different V^* *of* AGARD 445.6 *wing at* M_∞*=0.96,* ENFLOW *results in Euler mode*

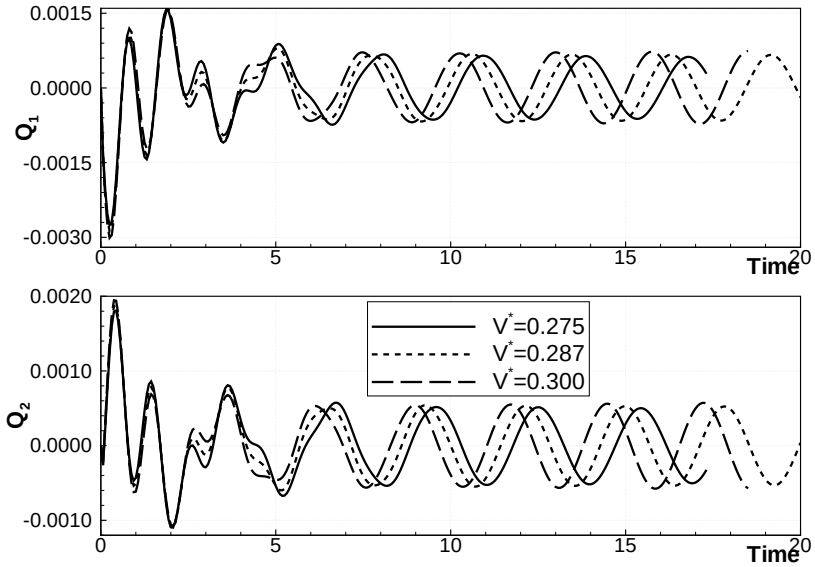

Fig. 17 Generalized force of the first and second mode at three different V^* of AGARD 445.6 *wing at M_∞=0.96,* ENFLOW *results in Euler mode*

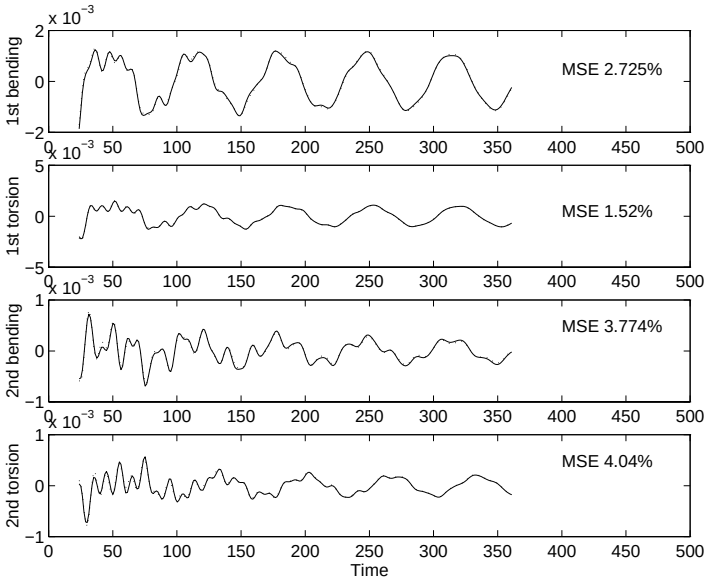

Fig. 18 Comparison of the generalized forces data between MIMO *fit (dotted line) based on the decoupled technique and real simulation (solid line) for* AGARD *aeroelastic system at subcritical flight condition (using* AESIM*)*

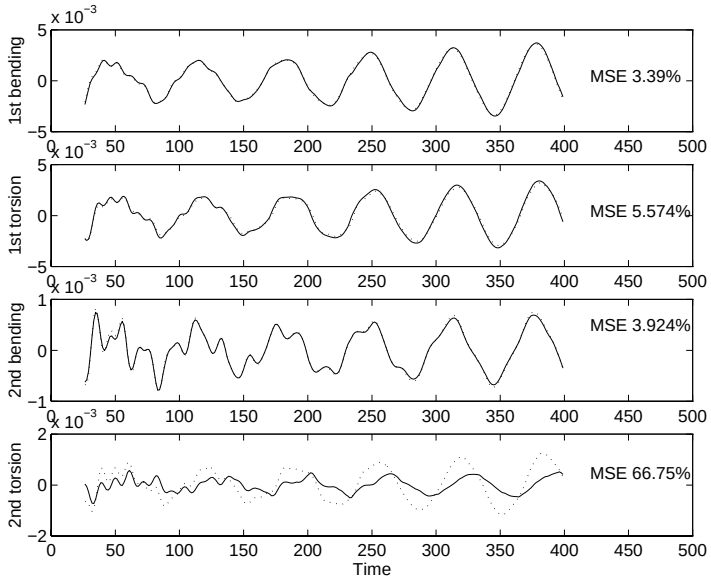

Fig. 19 Comparison of the generalized forces data between MIMO *prediction (dotted) based on the decoupled technique and real simulation (solid line) for* AGARD *aeroelastic system at supercritical flight condition (using* AESIM*)*